Guest-induced growth of a surface-basedsupramolecular bilayer

Matthew O. Blunt[1], James C. Russell[1], Maria del Carmen Gimenez-Lopez[2], Nassiba Taleb[2], Xiang Lin[2], Martin Schröder[2], Neil R. Champness[2]* and Peter H. Beton[1]*

[1]School of Physics and Astronomy, University of Nottingham, University Park, Nottingham NG7 2RD, UK, [2]School of Chemistry, University of Nottingham, University Park, Nottingham NG7 2RD, UK. *e-mail: peter.beton@nottingham.ac.uk; Neil.Champness@Nottingham.ac.uk

ABSTRACT

Self-assembly of planar molecules on a surface can result in the formation of a wide variety of close-packed or porous structures. Two-dimensional porous arrays provide host sites for trapping guest species of suitable size. Here we show that a non-planar guest species (C_{60}) can play a more complex role by promoting the growth of a second layer of host molecules (*p*-terphenyl-3,5,3˝,5˝-tetracarboxylic acid) above and parallel to the surface so that self-assembly is extended into the third dimension. The addition of guest molecules and the formation of the second layer are co-dependent. Adding a planar guest (coronene) can displace the C_{60} and cause reversion to a monolayer arrangement. The system provides an example of a reversible transformation between a planar and a non-planar supramolecular network, an important step towards the controlled self-assembly of functional, three-dimensional, surface-based supramolecular architectures.

INTRODUCTION

Two-dimensional molecular self-assembly at surfaces mediatedby weak, non-covalent interactions leads to the formation of networks with a wide variety of different forms and potential functionalities[1–3]. Reports of several examples of close-packed[4,5] and porous[6–9] structures on surfaces have a particular focus on the construction of templates capable of trapping guest molecular species[7,10–15]. In several cases guest molecules were shown to play a more complex role than simple passive occupation of voids within a network; instead, they actively promote transformations of the host framework between different two-dimensional configurations[16–18]. We report here the use of a non-planar guest that, when trapped in a two-dimensional framework on a surface, promotes a new mode of supramolecular growth into the third dimension perpendicular to the surface. Despite the extensive interest in the field of supramolecular templates, there are no previous examples of the growth of such networks perpendicular to the surface. The guest species, chosen as the fullerene C_{60} (2), has a near-spherical shape and simultaneously experiences stabilizing intermolecular interactions with molecules in both the first and second layer of a supramolecular bilayer. Furthermore, we find that the trapping of C_{60} and growth of the second layer of the supramolecular framework are co-dependent, which confirms a cooperative addition of host and guest species. Significantly, the growth of the bilayer network may be reversed subsequently by the addition of coronene, a planar molecule that displaces the C_{60} and destabilizes the bilayer structure, which leads to reversion to a monolayer arrangement. Overall, this system provides an example of a reversible transformation between a planar and a non-planar supramolecular network, an important step towards the controlled self-assembly of functional, three-dimensional, surface-based supramolecular architectures.

RESULTS AND DISCUSSION

Guest-induced perpendicular growth of a surface-based hydrogen-bonded network is observed following the addition of C_{60} (2) to an adsorbed monolayer of the molecule *p*-terphenyl-3,5,3˝,5˝-tetracarboxylic acid (TPTC, 1). The molecular structure of TPTC, shown in Fig. 1a, consists of a terphenyl backbone linked to four carboxylic acids. These side groups promote intermolecular hydrogen bonding and two possible relative placements of neighbouring molecules are stabilized by these interactions, as shown in Fig. 1a[6,17,19]. When adsorbed at the solid–liquid interface between highly oriented pyrolytic graphite (HOPG) and nonanoic acid (4), TPTC forms an extended monolayer array of hexagonal pores separated by 16.6 Å and stabilized by in-plane hydrogen bonding. A schematic of the resulting supramolecular monolayer is shown in Fig. 1b and in this paper we focus on the potential of the hexagonal pores to actas host sites for guest molecules[7,10–15].

An interesting feature of the TPTC monolayer structure isthat the pores are not all equivalent and we find a variation in the probability of trapping the guest molecules at different sites. The various hexagonal pores that combine to form the monolayer are shown in Fig. 1c (pores A–E). The pores are constructed from combinations of hydrogen-bonded dimers, as shown in Fig. 1a, and are composed of three (pore A), four (B, C), five (D) or six (E) molecules. The edges of these hexagonal units are formed either by the terphenyl backbone of TPTC (1) or by hydrogen-bonded junctions between carboxylic acid groups, which for this particular molecule have approximately equal lengths so that all the hexagonal pores (A–E) have, to a good approximation, equal dimensions. TPTC monolayers were investigated previouslyusing scanning tunnelling microscopy (STM), and imagessimilar to those published previously[6] are included in the Supplementary Information.

To investigate the possible capture of guest molecules, we first formed a TPTC monolayer on freshly cleaved HOPG (see Supplementary Information for full experimental details), andthen added a small quantity of a saturated solution of C_{60} in nona-noic acid (4). The STM image of the resultant HOPG–solution interface (Fig. 1d) shows the network structure obtained approxi- mately 24 hours after the addition of the C_{60} solution. The bright features in Fig. 1d correspond to individual C_{60} molecules sited within pores with a minimum C_{60}–C_{60} distance measured as $\sim$16.5 Å, in good agreement with the measured pore–pore spacing of the TPTC network[6]. This suggests that C_{60} adsorption occurred in some, but not all, of the pores in the TPTC network. In Fig. 1d ~53% of the pores are occupied by C_{60}.

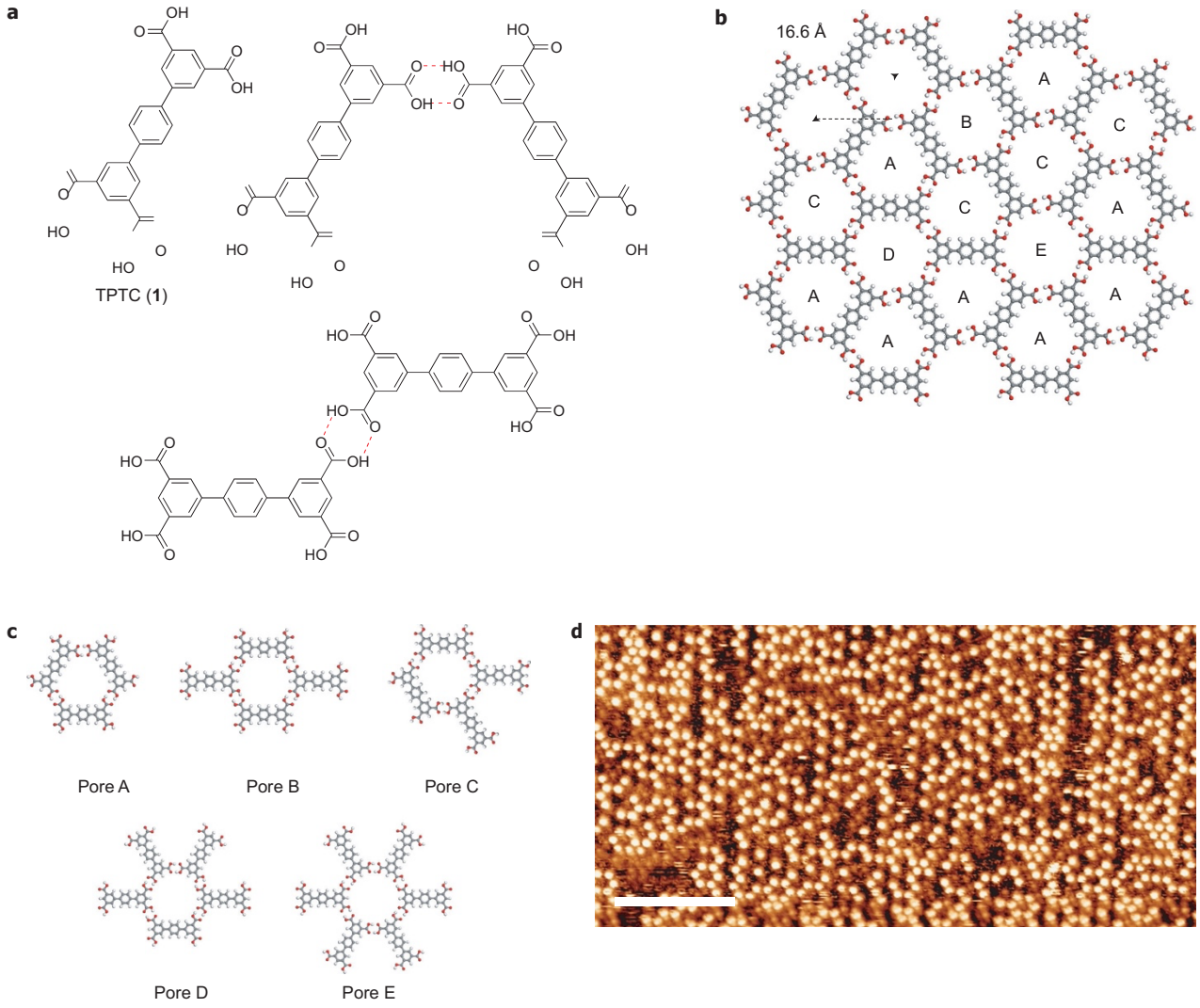

Figure 1 | Molecular structure of TPTC single-layer network. a, Molecular structure of TPTC and arrangements for hydrogen-bonded TPTC dimers with either the long axes of molecules mutually parallel or with one molecule rotated by 60°. b, Molecular schematic of a section of TPTC network that highlights the hexagonally ordered network of pores. The pore–pore separation (16.6 Å) is shown at the top left. c, Five possible arrangements of molecules that surround each pore within the TPTC network. The arrangements contain either three (pore A), four (pores B and C), five (pore D) or six (pore E) molecules. Examples of each of these pore types are labelled in (b). d, STM image of an area of TPTC network ~24 hours after deposition of C_{60}. The locations of C_{60} are clearly visible as the bright spots in the image; the underlying TPTC network structure is not visible. Scale bar ¼ 160 Å.

Although Fig. 1d shows the locations of the C_{60} molecules it contains little information about the arrangement of the TPTC molecules that surround them. Using a defect in the HOPG substrate as a nucleation site, the growth of a small area of the C_{60}–TPTC network was tracked through sequential STM images. The STM images in Fig. 2 show a large, bright feature that corresponds to a HOPG surface defect. Growing outwards from this defect is an area of adsorbed C_{60} molecules surrounded by a TPTC network. In the area where the C_{60} molecules are adsorbed the TPTC molecules are visible as bright, rod-like features. As we show below this high contrast arises because these molecules are in the upper layer of a TPTC bilayer structure. In the areas that surround the adsorbed C_{60} we observed a lower contrast layer, which corresponds to a TPTC monolayer adsorbed directly on graphite. The bilayer is fragile and regions can be removedby the STM tip, with subsequent regrowth (see Supplementary Information for examples).

A topographic cross-section through one of the STM scans is shown in Fig. 2b (the green line on Fig. 2c shows its location in the image). This cross-section confirms that a bilayer of TPTC was formed because the molecules in the monolayer have a significantly lower apparent height (1 Å) than the TPTC molecules that directly surround the adsorbed C_{60} (2.5 Å). The peak height of a C_{60} molecule is also shown on the cross-section (6.5 Å) and is in good agreement with previously reported values for C_{60} , as recorded by STM[20]. These apparent heights include contributions from variations in the local density of states and, therefore, differ from simple estimates of molecular dimensions. The apparent heights observed in the STM images indicate that the TPTC (1) molecules in the region close to the adsorbed C_{60} (2) form part of a second, overlying layer of TPTC network, which confirms the presence of a bilayer structure. We stress that neither C_{60} adsorption nor second-layer TPTC growth is observed in isolation, which indicates a co-dependence of these processes. The role of the guest molecule and the co-dependence of C_{60} inclusion and of TPTC bilayer formation distinguish the current study from previous examples of surface bilayer growth[21].

The adsorption sites in the TPTC monolayer that capture C_{60} may be determined by monitoring the growth of the bilayer structure. The three STM images in Fig. 2d–f track the growth that originated from the HOPG substrate defect in Fig. 2a. Once incorporated into the C_{60}–TPTC bilayer the C_{60} molecules, apart from a

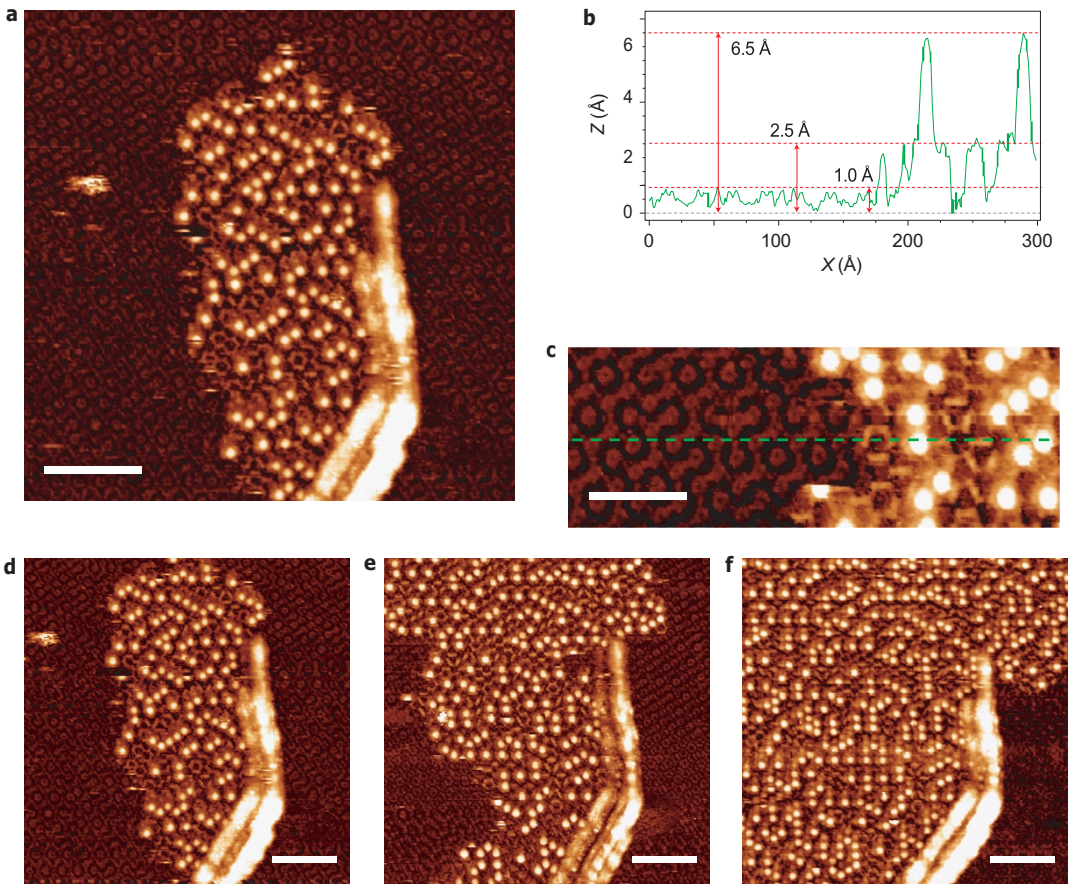

Figure 2 | Growth of the TPTC–C_{60} bilayer. a, STM image of TPTC network immediately after C_{60} deposition. An island of C_{60} and bilayer TPTC network grows outwards from a surface defect. The initial layer of TPTC network is visible with an altered contrast (see Supplementary Information) and the TPTC molecules in the second layer appear with the long axis of the molecules as bright, rod-like features. Scale bar ¼ 110 Å. b,c, Height profile (Z) taken through the edge (X) of the bilayer–C_{60} island (b). The location of the height profile is marked with a green dashed line on the magnified STM image (c). Scale bar ¼ 60 Å. d–f, STM images that show the growth of the bilayer–C_{60} island; the time between images is approximately five minutes. All images were acquired with a tunnelling current of 20 pA and a tip bias of þ1.2 V. Scale bars ¼ 100 Å.

few exceptions, remained in fixed locations and can be used as reference points to map accurately the registry between the C_{60} and the TPTC monolayer. The outer regions of the STM image shown in Fig. 2a were used to determine the configuration of TPTC molecules in the uncovered initial network layer. Using this approach we determined the molecular configuration of pores in the TPTC monolayer that later trap C_{60} molecules in the final bilayer structure. The results from this analysis are summarized in Table 1, in which the first row shows the fractional occurrence of pore types (A–E, see Fig. 1c) for the TPTC monolayer regions and the second row shows the fraction of trapped C_{60} in eachpore type. The results show a strong preference for adsorption in pores of type A, which make up 40% of pores in the initial layerbut 76% of pores that trap a C_{60} molecule. All other pores show a lower-than-expected C_{60} trapping occupancy (Table 1).

Also tabulated is the trapping energy for C_{60} in each pore type of a TPTC monolayer calculated using molecular dynamics, using a previously reported method for carboxylic acids on HOPG (see Supplementary Information for details). There is a clear correlation between capture probability (ratio of pore occurrence to occupation fraction (Table 1)) and calculated binding energy, with the most stable configuration being a C_{60} trapped in pore A (22.20 eV) and the least stable a C_{60} trapped in pore E (21.98 eV). The variations in binding energy arise from the differences in the internal dimensions of the pores. Edges that consist of a TPTC backbone protrude slightly into the pore, which gives rise to increased van der Waals interactions. Type A pores have the largest number of terphenyl edges and thus the smallest internal size and highest binding energy.

Figure 3 shows the overall structure, in cross-section (Fig. 3a) and top view (Fig. 3b), of a fullerene captured in type A pores in layers 1 and 2. The spherical shape of the fullerene cage means that the footprint of C_{60} on the graphite surface is smaller than its molecular diameter. Furthermore, the cross-sectional area of intersection between the fullerene and TPTC molecules is different in the planes of layer 1 and layer 2 molecules. Consequently, we would expect the C_{60}–TPTC interactions to have different strengths for the two layers. In fact, our calculations show that the fullerene is

Table 1 | Pore configurations – details of TPTC monolayers that trap C_{60} molecules.

	A	B	C	D	E
Fractional occurrence of TPTC monolayer pores (%)	40	2.9	27	19	9.2
Fraction of C_{60} trapped in each pore type (%)	76	1.6	15	6.2	1.1
Ratio of C_{60} trapped to fractional currence	1.9	0.6	0.6	0.3	0.1
Calculated trapping energy (eV) of C_{60} guests in pores in a single-layer TPTC on HOPG	22.20	22.10	22.11	22.05	21.98

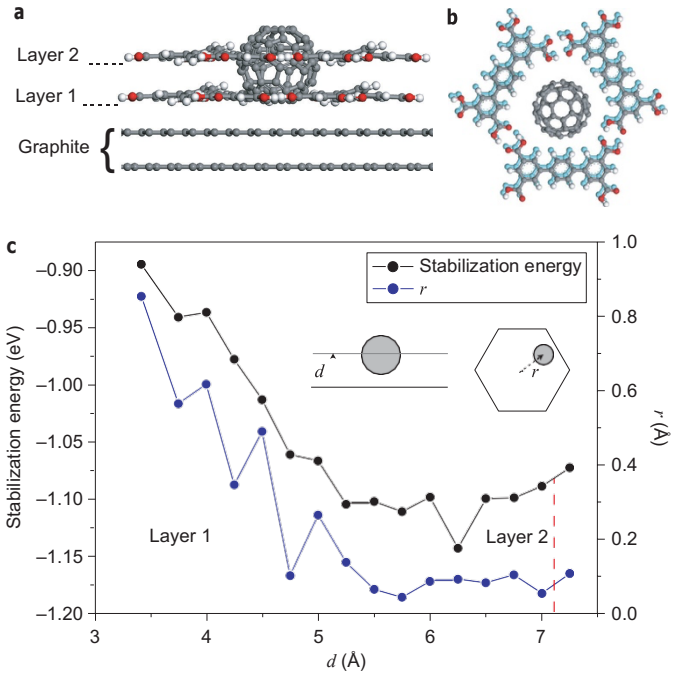

Figure 3 | Structure of TPTC–C_{60} bilayer. a, Side-view of the C_{60}–bilayer network that consists of two overlying pores of type A. b, A top view of this arrangement with the C_{60} placed at its minimum-energy position for both the first- (light blue) and second-layer pores (grey). The two layers are displaced slightly with respect to each other, which aids clarity, but in addition is expected on the basis of calculations (see text). c, Variation in stabilization energy and position for a C_{60} in a single-layer pore of type A when the vertical position of the pore is varied from the equilibrium position for a first-layer pore (3.4 Å) up to just above that for an equilibrium position for a second-layer pore (7.25 Å). Red dashed lines show the equilibrium vertical positions for layers 1 and 2.

stabilized in a non-central position within a hexagonal TPTC monolayer pore and is offset by a displacement, *r*, towards a hydrogen-bond type of edge. The value of *r* depends on *d*, the vertical offset between the graphite surface and the plane of the TPTC mol- ecules (see inset to Fig. 3c).

In Fig. 3c the calculated values for *r* and *E* (the interaction energy between the TPTC pore and the fullerene (interactions with the graphite surface are not included in this value)) are plotted against *d* for pore A. We find that for *d* 3.4 Å, which corresponds to the height of a TPTC monolayer, the displacement *r* is 0.8 Å, whereas for a second-layer TPTC, for which *d* 7.1 Å and *r* 0.1 Å. Analogous results for pores B–E are included in the Supplementary Information and show that as the number of terphe- nyl edges is reduced the trapping energy is lowered and the displa- cement *r* is increased. These results imply a relative lateral displacement of 0.6 Å between layer 1 and layer 2 framework mol-ecules if interactions are maximized in both layers simultaneously, although such a small offset cannot be determined directly fromour images because of the resolution limitations.

It is also possible to use the growth sequence in Fig. 2 to analyse the positions of second-layer TPTC molecules relative to the first layer, and in particular to determine whether there is a preference for the adsorption of a terphenyl over another terphenyl or a hydrogen-bonded edge (this analysis does not include second-layer TPTC molecules directly adjacent to fullerene guests, for which STM tip convolution leads to limited resolution). Our results indicate that there is no preferred configuration and the distribution is consistent with random placement. Further details are provided in the Supplementary Information and our results show no evidence for a strong interaction between colocated oxygen atoms in the two layers. It is also interesting to consider why similar systems into which C_{60} is introduced as a guest do not lead to bilayer or multilayer growth. In previous studies[10,19], C_{60} was captured in a pore of type E and the analogous three-dimensional/bilayer growth would require a direct stacking of pores of this type. In the TPTC network studied here a bilayer can be formed without the

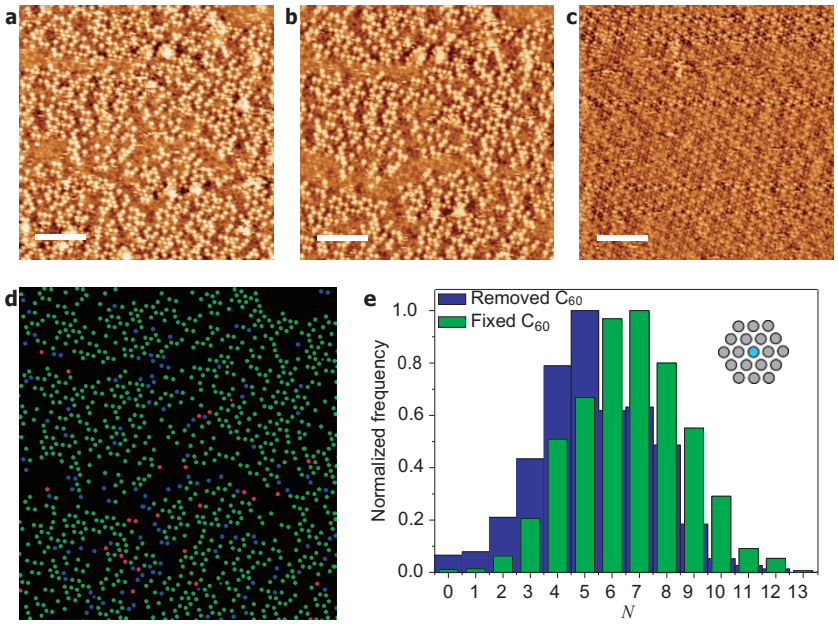

Figure 4 | Reversal of bilayer formation by the addition of coronene. a–c, Removal of the bilayer by coronene. Image (a) was taken approximately 20 minutes after the addition of the coronene solution, and images (b) and (c) after 40 and 60 minutes, respectively. Scale bars 160 Å. d, Schematic view that shows the C_{60} locations in (a) and (b). C_{60} molecules that remain fixed in place between (a) and (b) are coloured green, removed C_{60} molecules (those present in (a) but not in (b)) are coloured blue and recaptured C_{60} molecules (those present in (b) but not in (a)) are coloured red. e, Histograms that detail the distribution of coordination number *N* (number of occupied nearest-neighbour and next nearest-neighbour sites, see inset) for fixed C_{60} (green) and removed C_{60} (blue).

requirement to stack such pores – indeed, this structure is statisti- cally unlikely because of the low occurrence and occupancy of type E pores. A possible explanation is that such stacking is energe- tically unfavourable and inhibits fullerene-mediated multilayer for- mation in trimesic acid and related supramolecular arrays[10,19].

The formation of the bilayer TPTC–C_{60} network can be reversed by the addition of coronene (3) as a second guest molecule. Figure 4a–c shows STM images taken 20 (Fig. 4a), 40 (Fig. 4b)and 60 (Fig. 4c) minutes, respectively, after the addition of 10 mlof a solution of coronene in nonanoic acid (4) (0.0015 mg ml^{21}) to the sample. After the addition of coronene, the bilayer–C_{60} network was replaced by a single-layer TPTC network with coro- nene immobilized within its pores (coronene is trapped preferen- tially in pores of type E, as demonstrated previously by Griessl*et al.*[22]). Initially, this process proceeded relatively slowly with a reduction in the number of C_{60} molecules of 10% in 20 minutes (Fig. 4a and Fig. 4b). However, after 40 minutes (Fig. 4c) the C_{60}– bilayer structure was removed completely, which suggests asudden onset of removal of C_{60} and the absorption of coronene.

The removal of C_{60} is non-random and displays spatial corre- lations, as shown in Fig. 4d in which the positions of fullerene molecules removed between the acquisitions shown in Fig. 4a,b are highlighted (removed molecules are blue, fixed molecules are green—a small number of newly trapped C_{60} appeared and are marked red). This mapping shows that the initial fullerene adsorption is concentrated in small islands with lateral dimensions 250 Å, around which there are boundaries where no fullerene adsorption occurs. This is consistent with islands of fullerene–TPTC nucleating at separate sites and growing into small, disconnected domains. The removal of C_{60} guests (blue) is concentrated at the edge of these domains, as confirmed by a histogram (Fig. 4e) of the coordi-nation numbers (N, the number of nearest-neighbour and next nearest-neighbour sites occupied by a C_{60}) that remain fixed (green) or are removed (blue). The histogram peak is at a lower value, N 5, for the removed molecules than for the fixed molecules (peak at N 7). This implies that the coronene- induced, second-layer removal occurred at domain edges in a reversal of a growth process. Interestingly, the occurrence of such domains indicates that a second-layer island nucleated in a TPTC monolayer does not continuously join an island nucleated at a different site. This suggests that second-layer islands nucleated at different sites can have variations in their registry with the first TPTC layer. Thisis consistent with the non-central adsorption site of the C_{60} discussed above, which leads to at least six non-equivalent registries of the bilayer.

The demonstration that non-planar guest molecules may be used to promote the formation of supramolecular bilayers opens up a wide range of new possibilities for the formation of functional three-dimensional supramolecular architectures. The reversible nature of the growth process highlights the delicate balance of inter- actions required for perpendicular growth and provides an example of a responsive system in which guest exchange leads to changes in dimensionality.

REFERENCES

1. Bartels, L. Tailoring molecular layers at metal surfaces. *Nature Chem.* 2, 87–95 (2010).
2. Elemans, J. A. A. W., Lei, S. B. & De Feyter, S. Molecular and supramolecular networks on surfaces: from two-dimensional crystal engineering to reactivity. *Angew. Chem. Int. Ed.* 48, 7298–7332 (2009).
3. Barth, J., Costantini, G. & Kern, K. Engineering atomic and molecularnanostructures at surfaces. *Nature* 437, 671–679 (2005).
4. Adisoejoso, J. *et al*. Two-dimensional crystal engineering: a four-componentarchitecture at a liquid–solid interface. *Angew. Chem. Int. Ed.* 48, 7353–7357 (2009).
5. Chen, W. *et al*. Two-dimensional pentacene: 3,4,9,10-perylenetetracarboxylic dianhydride supramolecular chiral networks on Ag(111). *J. Am. Chem. Soc.* 130, 12285–12289 (2008).
6. Blunt, M. O. *et al*. Random tiling and topological defects in a two-dimensionalmolecular network. *Science* 322, 1077–1081 (2008).
7. Theobald, J. A., Oxtoby, N. S., Phillips, M. A., Champness, N. R. & Beton, P. H.Controlling molecular deposition and layer structure with supramolecular surface assemblies. *Nature* 424, 1029–1031 (2003).
8. Stepanow, S. *et al*. Surface-assisted assembly of 2D metal–organic networks that exhibit unusual threefold coordination symmetry. *Angew. Chem. Int. Ed.* 46, 710–713 (2007).
9. Tahara, K. *et al*. Two-dimensional porous molecular networks of dehydrobenzo[12]annulene derivatives via alkyl chain interdigitation. *J. Am.Chem. Soc.* 128, 16613–16625 (2006).
10. Griessl, S. J. H. *et al*. Room-temperature scanning tunneling microscopy manipulation of single C_{60} molecules at the liquid–solid interface: playingnanosoccer. *J. Phys. Chem. B* 26, 11556–11560 (2004).
11. Madueno, R., Raisanen, M. T., Silien, C. & Buck, M. Functionalising hydrogen- bonded surface networks with self-assembled monolayers. *Nature* 454, 618–621 (2008).
12. Ivasenko, O. *et al*. Supramolecular assembly of heterocirculenes in 2D and 3D. *Chem. Commun.* 1192–1194 (2009).
13. Schull, G. *et al*. Selectivity of single-molecule dynamics in 2D molecular sieves. *Adv. Mater.* 18, 2954–2957 (2006).
14. Wahl, M., Stohr, M., Spillmann, H., Jung, T. A. & Gade, L. H. Rotation–libration in a hierarchic supramolecular rotor–stator system: Arrhenius activation and retardation by local interaction. *Chem. Commun.* 1349–1351 (2007).
15. Stepanow, S. *et al*. Steering molecular organization and host–guest interactions using two-dimensional nanoporous coordination systems. *Nature Mater.* 3, 229–233 (2004).
16. Wu, D., Deng, K., He, M., Zeng, Q. & Wang, C. Coadsorption-induced reconstruction of supramolecular assembly characteristics. *ChemPhysChem* 8,1519–1523 (2007).
17. Blunt, M. *et al*. Directing two-dimensional molecular crystallisation using guesttemplates. *Chem. Commun.* 2304–2306 (2008).
18. Li, M. *et al*. Site-selective fabrication of two-dimensional fullerene arrays by using a supramolecular template at the liquid–solid interface. *Angew. Chem. Int.Ed.* 120, 6819–6823 (2008).
19. Zhou, H. *et al*. Frustrated 2D molecular crystallization. *J. Am. Chem. Soc.* 129, 13774–13775 (2007).
20. Keeling, D. L., Humphry, M. J., Moriarty, P. & Beton, P. H. Attractive mode manipulation of covalently bound molecules. *Chem. Phys. Lett.* 366, 300–304 (2002).
21. Samorì, P., Severin, N., Simpson, C. D., Müllen, K. & Rabe, J. P. Epitaxial composite layers of electron donors and acceptors from very large polycyclic aromatic hydrocarbons. *J. Am. Chem. Soc.* 124, 9454–9457 (2002).
22. Griessl, S. J. H. *et al*. Incorporation and manipulation of coronene in an organictemplate structure. *Langmuir* 20, 9403–9407 (2004).

ACKNOWLEDGEMENTS

We thank the UK Engineering and Physical Sciences Research Council for financial support under grant EP/D048761/1. M.S. thanks the European Research Council for an Advanced Grant. N.R.C. acknowledges the receipt of a Royal Society Leverhulme Trust Senior Fellowship.

AUTHOR CONTRIBUTIONS

M.O.B. and J.C.R. acquired the STM data, M.O.B. performed the MD simulations, M.C.G, X.L., M.S. and N.R.C. developed the synthetic route for the TPTC molecule, M.O.B. and P.H.B. analysed the data, M.O.B., N.R.C. and P.H.B. conceived and coordinated the experimental work and M.O.B., N.R.C. and P.H.B. co-wrote the paper.

ADDITIONAL INFORMATION

The authors declare no competing financial interests. Supplementary information and chemical compound information accompany this paper at www.nature.com/ naturechemistry. Reprints and permission information is available online at http://npg.nature.com/reprintsandpermissions/. Correspondence and requests for materials should be addressed to N.R.C. and P.H.B.

Supplementary information

1) Molecular synthesis:

TPTC (1) was prepared from the oxidation of 3,5,3”5”-tetramethyl-p-terphenyl, 2, see Scheme 1.

Scheme 1: Suzuki coupling reaction of 2,6-dibromobenzene with 3,5-dimethylphenylboronic acid followed by oxidation of the methyl groups to give 1.

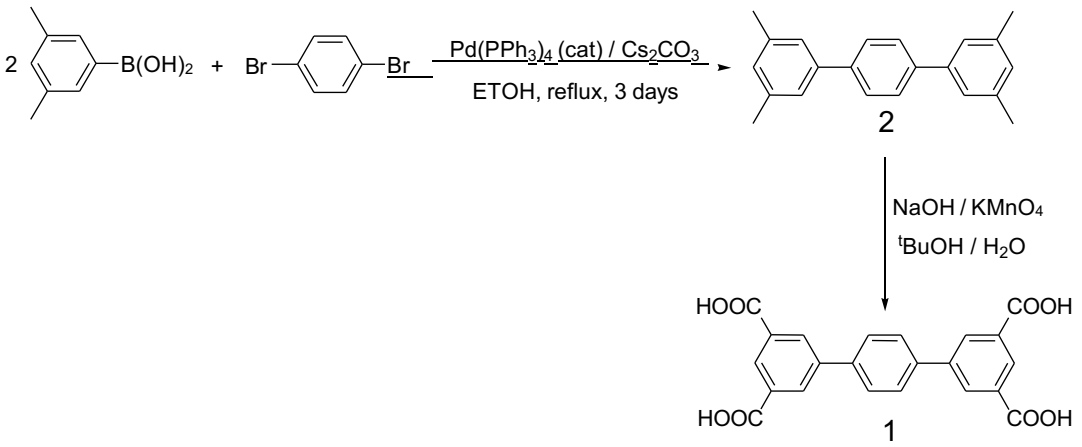

3,5,3”5”-tetramethyl-p-terphenyl (2)

2,6-Dibromobenzene (378 mg, 1.6 mmol), an excess of 3,5-dimethylphenylboronic acid (600 mg, 4 mmol) and Cs_2CO_3 (1.4 g, 4 mmol) were mixed in EtOH (10 ml), and the mixture de-aerated using N_2. $Pd(PPh_3)_4$ (18.5 mg, 1% of 1.6 mmol) was added to the reaction mixture with stirring and the mixture refluxed at 80°C for 3 days under N_2. The reaction mixture was evaporated to dryness, and the residue extracted into $CHCl_3$ and washed with water. The organic layer was dried over $MgSO_4$ and the solvent was removed under reduced pressure to provide a crude product which was purified by silica gel chromatography using hexane as eluent. The product was obtained as a colourless crystalline solid. Yield: 328 mg, 75%. ^{1}H NMR (acetone-d^6, 270MHz): 7.73 (s, 4H), 7.33(s, 4H), 7.03(s, 2H), 2.38 (s, 12H). ^{13}C NMR (acetone-d^6, 270MHz): δ 140.87, 140.24, 138.37, 129.01, 127.48, 125.05, 21.523. EI-MS (m/z) found: 287.1807 ($[M+H]^+$, 100%). Elemental analysis (% calc/found) for $C_{22}H_{22}$: C 92.26/92.33, H 7.74/7.73.

Synthesis of p-terphenyl-3,5,3´5´-tetracarboxylic acid (TPTC) (1)

3,5,3',5'-Tetramethyl-p-terphenyl (171 mg, 0.6 mmol) and NaOH (381 mg, 9.5 mmol) were dissolved in t-BuOH:water (16 mL, 1:0.6). The reaction was heated to 55°C and $KMnO_4$ (1.12 g, 7.1 mmol) was added in portions over 2 days and the reaction was stirred at 55ºC until completion of the oxidation process. EtOH was added to the mixture to destroy excess $KMnO_4$, and the mixture heated to 90°C. The MnO_2 precipitate was removed by filtration and the filtrate concentrated under vacuo. Concentrated HCl was added dropwise with stirring until no more white precipitate formed (pH = 2). The product was collected by centrifugation, washed with water to remove excess acid and then with acetone and dried in vacuo. Yield: 100 mg, 41 %. ^{1}H NMR (DMSO-d^6, 270MHz): 8.48 (t, 2H, J=1.53 Hz), 8.45 (d, 4H, J=1.53 Hz), 7.92 (s, 4H). ^{13}C NMR (acetone-d^6, 270MHz): δ 167.07, 140.82, 138.73, 132.86, 131.72, 129.58, 128.32. EI-MS (m/z) found: 405.0609 ($[M+H]^-$, 100%), 361.0752 ($[M-H-(COOH)]^-$, 82.6%). Elemental analysis (% calc/found) for $C_{22}H_{14}O_8$: C 65.03/64.95, H 3.47/3.43.

2) Experimental details:

STM experiments were carried out on an Agilent Technologies 4500 PicoPlus STM using a PicoScan controller. STM tips were formed from mechanically cut 80:20 PtIr wire and substrates were freshly cleaved highly oriented pyrolytic graphite (HOPG). Nonanoic acid (>95%), C_{60} (fullerene powder sublimed 99.92%) and coronene (>99%) were used as purchased from Fluka, Alfa Aesar and Sigma-Aldrich, respectively.

Saturated solutions of C_{60} and TPTC both in nonanoic acid were prepared by placing an excess of solid in the solvent and using ultrasonic agitation to ensure complete saturation of the solution. HOPG surfaces were mechanically cleaved prior to each experiment to ensure a clean substrate. In order to form TPTC networks a 10μL droplet of TPTC in nonanoic solution was deposited on to an HOPG surface with imaging commencing immediately using the STM tip. Once imaging of the TPTC network was complete the tip was withdrawn and a further 10μL droplet of C_{60} in nonanoic acid solution was added to the liquid cell. The tip was then re-engaged and imaging commenced. After imaging the bilayer network structure the tip was withdrawn again and 10μL of coronene in nonanoic acid solution (0.0015mg/mL) was added to the liquid cell, and this was followed by further imaging.

3) Image analysis and processing:

3.1 Trapping of C_{60} in bilayer network

The STM images in Fig. 1 (main paper) show distinctive imaging contrasts which represent a single layer TPTC network as a mazelike network and the second layer as bright rod-like features. Fig. S1 shows examples of both of these imaging contrasts for a single layer TPTC network. That both of these contrasts can be obtained for a monolayer of TPTC highlights the fact that the imaging contrast is closely related to the detailed nature of the tip termination. The exact termination of the tip is unknown and can vary with adsorption/desorption of molecules or by re-arrangement of the atomic structure of the tip apex. Our lack of knowledge concerning the exact nature of the tip apex makes it difficult to account for these differences from a fundamental perspective. It should be noted however that for the bilayer arrangement we only observe the 'rod-like' imaging contrast for the second layer of TPTC molecules and that both these distinct contrasts, 'maze-like' for the first layer and 'rod-like' for the second, are observed within a single scan. The presence of both imaging contrasts within a single scan (and therefore with a constant tip termination) suggests that differences in the environment of the two layers, for example their coupling to the substrate, may be responsible for the observed imaging differences.

We are able to identify the orientation of each of the TPTC sub-units in images of networks with either the maze, or rod-like contrast. Fig. S2 shows examples of how distinct features in the maze-like imaging contrast correspond to the different configurations of TPTC molecules in the five different pore types (A-E, see Fig. S2). Using this scheme it is possible to take an image of a TPTC network which displays this contrast and map out the locations and orientations of the individual TPTC molecules. By mapping out the configuration of TPTC molecules in early images (Fig. 1f main paper), and then comparing this map to the locations of adsorbed C_{60} molecules in later images (Fig. 1h main paper) it was possible the define the molecular configuration of each first layer TPTC pore which subsequently trapped a C_{60} in the growing bilayer structure (see Table 1 main paper for statistics).

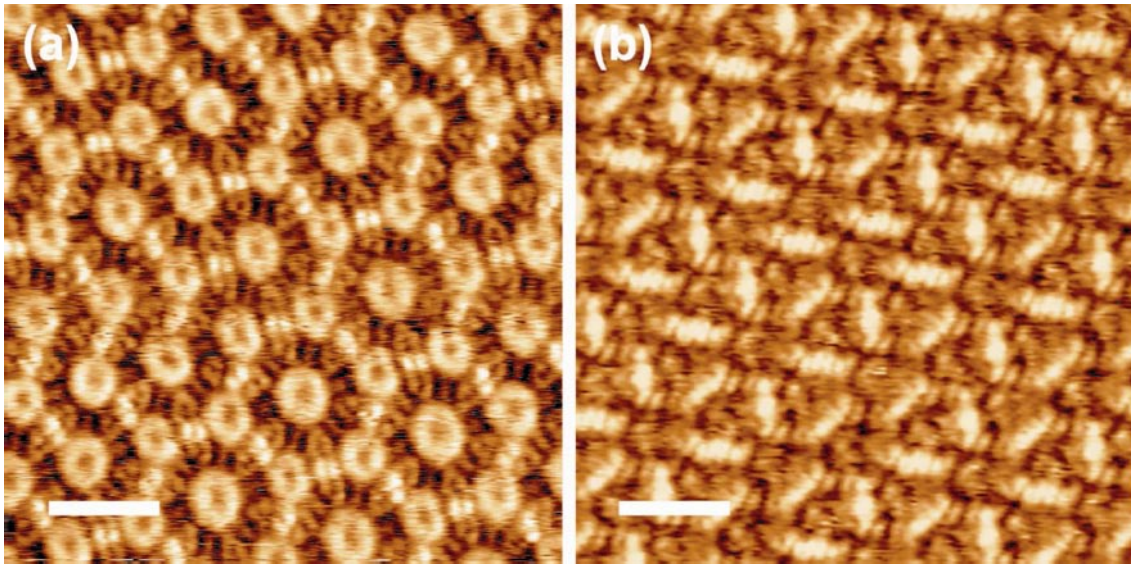

Fig. S1: a) and b) STM images of different regions of a single layer TPTC network, all scale bars:23 Å.

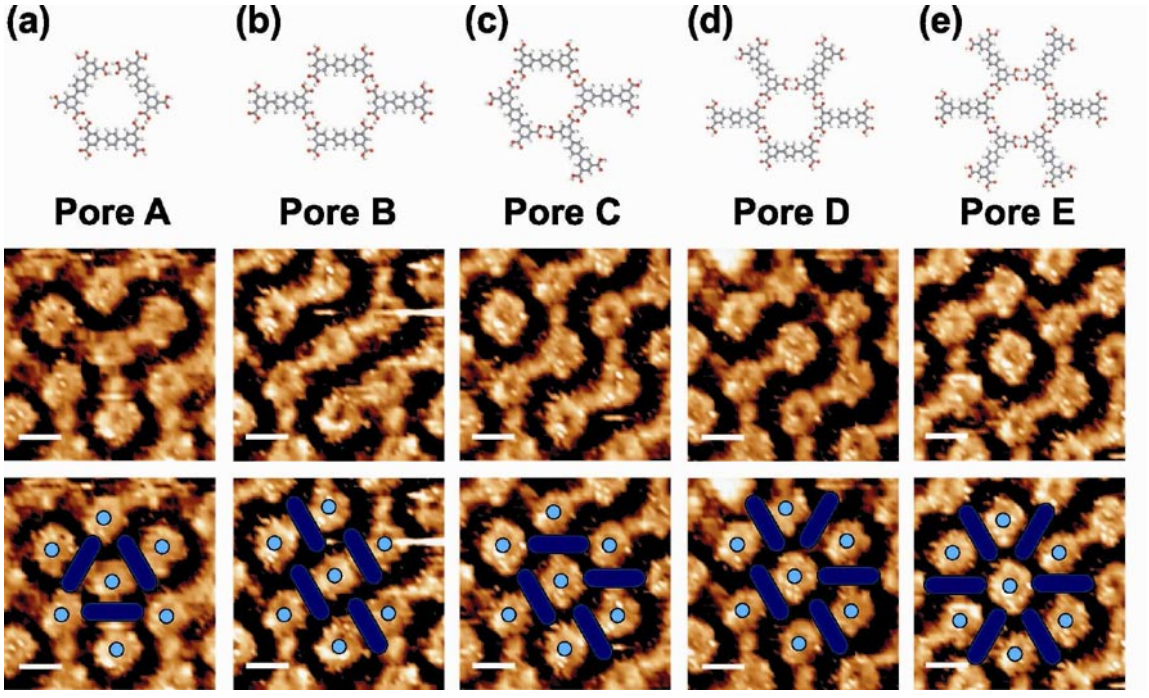

Fig. S2: a)-e) The molecular arrangement of the five different pore configurations (A-E). Below each of these is an example of that type of pore in an STM image which displays the mazelike imaging contrast. The final row of images shows the same STM images with the positions of the pores (light blue circles) and of the TPTC molecules (dark blue rectangles) marked. All scale bars: 10 Å.

3.2 The effect of tunneling parameters and the stability of the bilayer network

The stability of the bilayer network was found to be very closely related to the tunneling parameters. Imaging of the bilayer was possible only when using very small tunnel current values which were close to the noise limit of the system (<30pA) and over a narrow range of bias voltages (+1.0V to +1.3V applied to the tip). Moving outside this range of values caused a removal of the C_{60}/bilayer network leaving a monolayer of TPTC. Even when imaging within this small range of tunneling parameters regions of the bilayer network were occasionally removed and are subsequently re-grown. An example of this type of removal and re-growth is shown in Fig. S3.

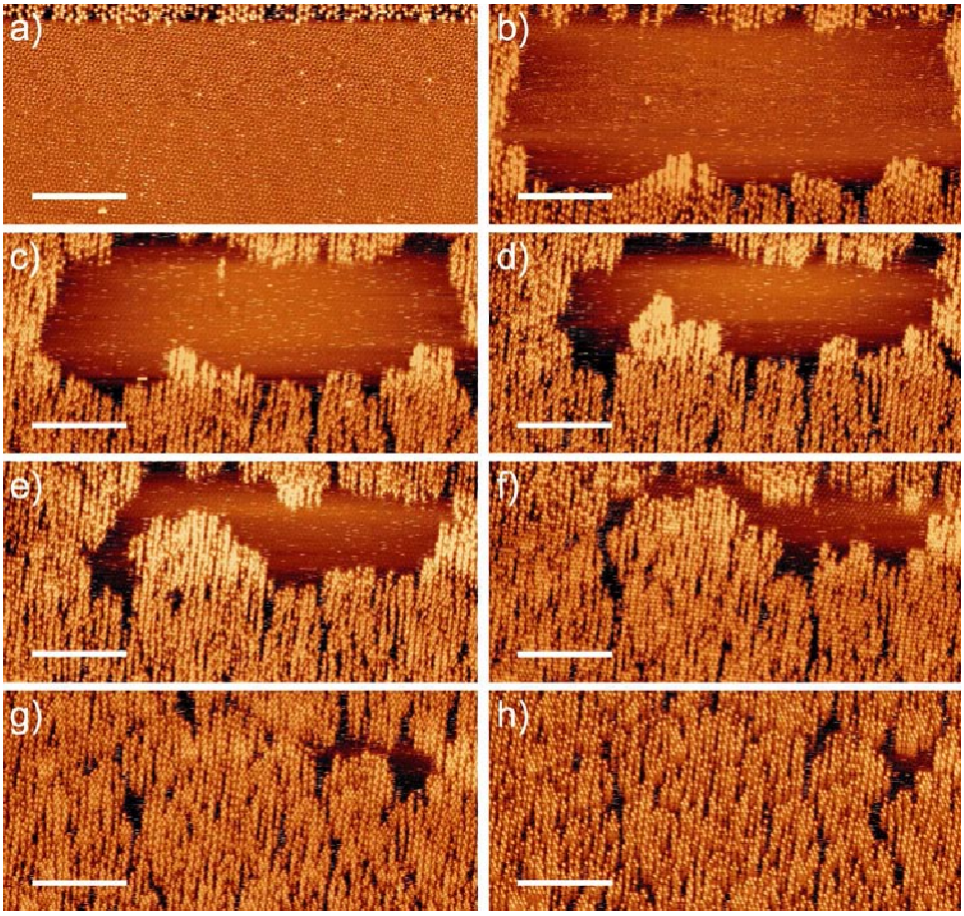

Fig. S3: Set of STM images showing the removal and re-growth of a region of C_{60}/bilayer network during scanning. a) Shows the removal of a region of bilayer network with only underlying monolayer of TPTC remaining visible. Images b) through h) show the subsequent re-growth of the C_{60}/bilayer network. All images were taken with the slow scan direction from bottom to top and at ~3min intervals. All images were obtained with a tunnelling current of 10pA and a tip bias of +1.2V. All scale bars 300 Å.

3.3 Positions of 2nd layer TPTC molecules

The images in Fig. 1 (main paper) have been analysed to identify the orientation and position of some of the 2nd layer TPTC molecules. In total 53 TPTC molecules in the 2nd layer could be analysed in this way (2nd layer molecules directly adjacent to a fullerene could not be clearly resolved).

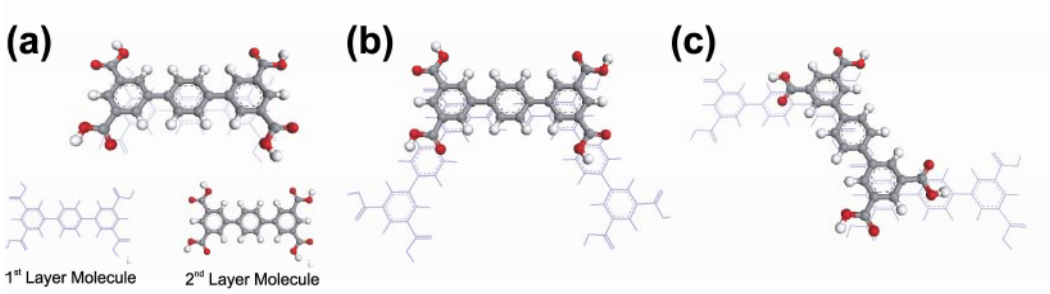

Fig. S4: Schematic showing the three possible positions for a second layer TPTC molecule. a) Directly on top of a molecule in the first layer, b) on top of a hydrogen bond between two non-parallel TPTC molecules and c) on top of a hydrogen bond between two parallel TPTC molecules in the first layer.

The coincidence of pore locations in the two TPTC layers constrains the number of positions a 2nd layer TPTC molecule can adopt with respect to first layer molecules to three possibilities. These arrangements are shown schematically in Fig. S4. There was an approximately equal distribution between second layer molecules adsorbed directly on top of another molecule (position A, 53%), or on top of a carboxylic acid…carboxylic acid hydrogen bond (positions B and C, 47%) (see Table S1). Of the second layer molecules adsorbed on top of a hydrogen bond, the distribution between position B (on top of a hydrogen bond between two non-parallel molecules) and position C (on top of a hydrogen bond between two parallel molecules) was 36% and 11%, respectively. This is very close to the distribution of non-parallel (B) and parallel (C) hydrogen bonds in the uncovered layer of TPTC network. These observations indicate that the orientation and position of TPTC molecules in the second layer are not affected by TPTC molecules in the first layer.

Table S1: Distribution of different positions adopted by second layer TPTC molecules relative to underlying TPTC molecules in the first layer.

A	B	C
28 (52.8%)	19 (35.9%)	6 (11.3%)

4) Molecular Mechanics and Molecular Dynamics simulations:

4.1 Molecular Modelling methodology

A series of molecular modelling simulations were carried out in order to calculate the stabilisation energy of a C_{60} molecule adsorbed as a guest in the different single layer pore configurations. Simulations were carried out using Materials Studio 4.4 and Forcite packages from Accelrys. The PCFF force field was used to assign atomic charges as well as to perform geometry optimisations[1]. A conjugate gradient algorithm was employed with an RMS force convergence parameter set to 10^{-2} kcal/mol.Å and the non-bonded van der Waals, and electrostatic terms both described by a spline function with a cut-off at 14.0 Å and a spline width of 3 Å.

To calculate the interactions between C_{60}, TPTC molecules and the underlying HOPG surface we used a method which has been reported previously both for calculating the adsorption energy of a closely related molecule on HOPG [2] and the stabilisation energy of coronene as a guest molecule in a porous hexa-isophthalic acid network.[3] A periodic cell containing a double layer of HOPG (30 HOPG lattice constants in size) was used for which all HOPG carbon atoms were constrained to fixed positions. Electrostatic interactions were treated using the Ewald technique (accuracy of 0.01 kcal/mol). Molecular dynamics simulations were performed in the canonical ensemble (N□V□T) at 298K with a Nosé-Hoover thermostat. The time step was set to 1 fs and the duration of the simulations to 300 ps with an output frame collected every 150 fs. In turn each of these output frames underwent a further geometry optimisation procedure. The lowest energy value found in this manner is used as the basis to calculate adsorption energies for the structure on the HOPG substrate and the stabilisation energy of a guest C_{60} molecule.

4.2 Pore configurations on HOPG

For each pore type (A-E) a molecular dynamics simulation was carried out to determine the lowest energy configuration for adsorption on the HOPG. In each case the resultant structures showed the individual TPTC molecules of the pore configurations rotated by 5.2° ± 0.1° with respect to the HOPG substrate (Fig. S5a shows an example structure for pore A).

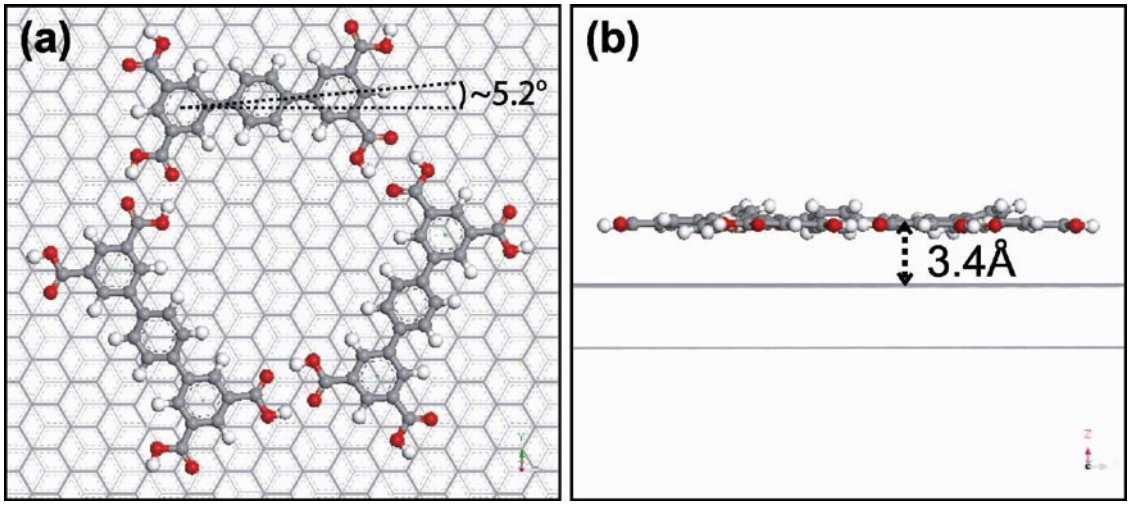

Fig. S5: a) An example of the output of the molecular dynamics simulation to calculate the lowest energy adsorption configuration for pore A on an HOPG substrate. The darker grey lines in the substrate represent the upper layer of the two layer slice of HOPG used in the simulation. b) The same structure from a side on view; the vertical height of the pore layer above the HOPG ~3.4 Å. This view highlights the slight rotation of the central benzene ring of each TPTC molecule.

The structure is predominantly planar and parallel to the underlying HOPG. However, the central benzene rings of each of the TPTC molecules are rotated slightly around the long axis of the molecule (Fig. S5b). This slight rotation of the central benzene ring in a TPTC occurs for all of the different pore configurations when adsorbed on HOPG. The vertical height from the HOPG substrate for single layer pores of all five types is ~ 3.4 Å. Similar simulations were also carried out to determine the height of the second TPTC layer in a bilayer arrangement, giving a vertical distance of ~7.1 Å from the upmost HOPG layer.

4.3 Stabilisation energy of C_{60} as a guest molecule.

The lowest energy configurations for the five different pore types on an HOPG surface were taken and all of the atoms in the TPTC molecules, apart from those of the central benzene ring, were constrained in the x, y and z directions (Fig. S6). This constraint was introduced to mimic the constrained nature of TPTC molecules in an extended network. The central benzene rings of the TPTC molecules were left unconstrained as the small rotations that they can undergo may effect the stabilisation energy of a C_{60} guest in the different pore structures. A single C_{60} molecule was then placed over the centre of each pore structure at a distance of 6.3 Å (measured from the

centre of the C_{60} molecule) above the upper HOPG layer. Following this, molecular dynamics simulations were carried out to find the lowest energy configuration for a C_{60} within the different pore types. By combining the energy values calculated for the empty pore structure on HOPG and that of the combination of the pore structure and a C_{60} guest molecule the stabilisation energies for C_{60} adsorbed in the different pore types was calculated. These stabilisation energy values are a combination of the interaction between the C_{60} and the underlying HOPG and the interaction between the C_{60} and the surrounding TPTC network (see Table 1 main paper).

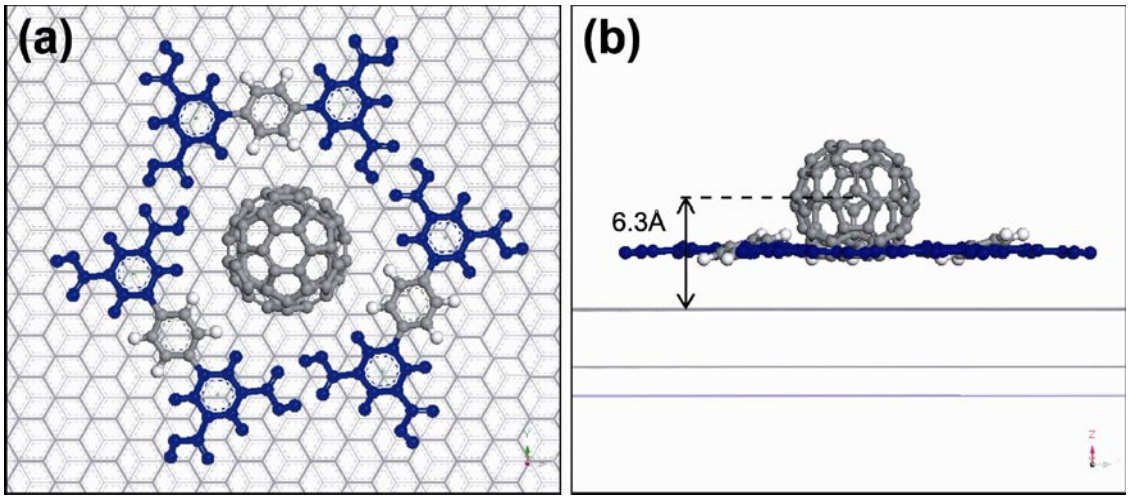

Fig. S6: a) Diagram showing the starting configuration for the molecular dynamics simulation to calculate the stabilisation energy for C_{60} as a guest molecule in a type A pore. The atoms coloured blue are not allowed to move in the x, y, and z directions to mimic the constrained nature that TPTC molecules would have in a true extended network. b) Side on view of the starting configuration the C_{60} molecule is initially placed in at a distance of 6.3 Å (as measured from the centre of mass of the C_{60} molecule) above the upper HOPG layer.

Using the same technique, stabilisation energies for C_{60} as a guest molecule in each of the single layer TPTC pores types was calculated for various vertical distances (d) of the pore layer above the HOPG substrate Along with the stabilisation energy, the horizontal distance (r) between the equilibrium position of C_{60} and the centre of the pore was also calculated. The results for these simulations are shown in Fig. S7.

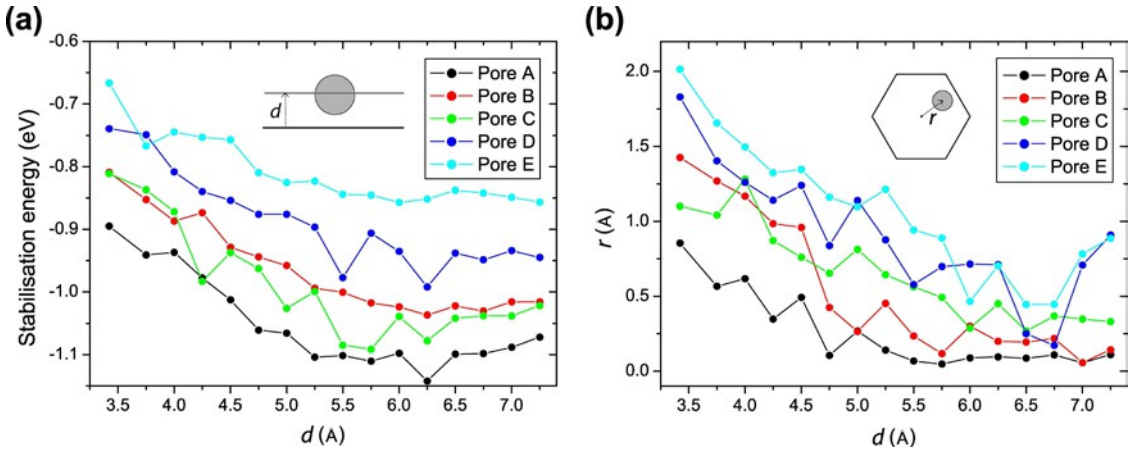

Fig. S7: a) Stabilisation energy for a C_{60} guest molecule in the five different single layer TPTC pore types vs vertical position of the single layer pore. b) Horizontal distance between the equilibrium C_{60} position and the centre of the single layer pore vs vertical position of pore. The insets to a) and b) show schematic descriptions of the variables d and r.

5 References

1. Sun, H.; Mumby, S. J.; Maple, J. R.; Hagler, A. T. An ab initio CFF93 all-atom force field for polycarbonates, J. Amer. Chem. Soc., 116, 2978-2987 (1994).
2. Zeigler, A., et al. Covalent template approach toward functionalized oligo-alkyl-substituted shape-persistent macrocycles: synthesis and properties of rings with a loop, Chem. Mater., 17, 5670-5683 (2005).
3. Lei, S., et al. Programmable hierarchical three-component 2D assembly at a liquid−solid interface: recognition, selection, and transformation, Nano. Lett., 8, 2541-2546 (2008).